Chem

CellPress

Article

An axial-to-axial chirality transfer strategy for atroposelective construction of C–N axial chirality

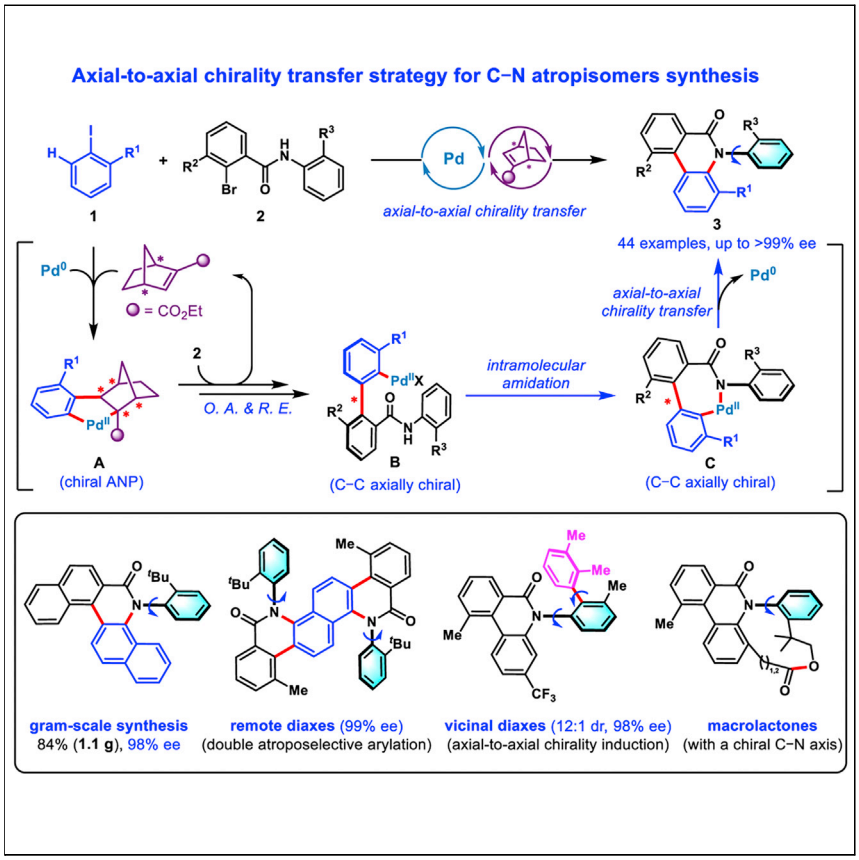

C–N axially chiral skeletons are prevalent in bioactive natural products and pharmaceuticals. However, their atroposelective synthesis remains a formidable challenge. Herein, an efficient method for the synthesis of C–N axially chiral phenanthridinones through palladium/chiral norbornene cooperative catalysis is reported. The strategy involves a unique axial-to-axial chirality transfer process, which has been scarcely reported. DFT calculations are performed to elucidate the reaction mechanism and the chirality transfer process, providing broader implications for future studies in asymmetric synthesis.

Ze-Shui Liu, Pei-Pei Xie, Yu Hua, ..., Hong-Gang Cheng, Xin Hong, Qianghui Zhou

hxchem@zju.edu.cn (X.H.)
qhzhou@whu.edu.cn (Q.Z.)

Highlights

Unique axial-to-axial chirality transfer for C–N axial chirality construction

Ability to assemble two vicinal and remote stereogenic axes

Step-economic and scalable synthesis of enantioenriched phenanthridinones

Broad scope, good yields, and excellent enantioselectivities

Liu et al., Chem 7, 1–16
July 8, 2021
https://doi.org/10.1016/j.chempr.2021.04.005

Please cite this article in press as: Liu et al., An axial-to-axial chirality transfer strategy for atroposelective construction of C–N axial chirality, Chem (2021), https://doi.org/10.1016/j.chempr.2021.04.005

Chem

CellPress

Article

An axial-to-axial chirality transfer strategy for atroposelective construction of C–N axial chirality

Ze-Shui Liu,[1,4] Pei-Pei Xie,[2,4] Yu Hua,[1] Chenggui Wu,[1] Yuanyuan Ma,[1] Jiangwei Chen,[1] Hong-Gang Cheng,[1] Xin Hong,[2,3,*] and Qianghui Zhou[1,5,*]

SUMMARY

C–N axially chiral skeletons are ubiquitous in bioactive natural products, pharmaceuticals, and chiral ligands. However, their atroposelective synthesis remains a formidable challenge because of their innate low configurational stability compared with that of well-developed C–C atropisomers. Herein, we report a general and efficient method for accessing C–N atropisomers through an axial-to-axial chirality transfer strategy based on palladium/chiral norbornene cooperative catalysis. The obtained C–N axial chirality originates from the preformed transient C–C axial chirality with high fidelity. A variety of C–N axially chiral phenanthridinones are obtained in excellent enantioselectivities (44 examples, up to >99% ee). This method can be applied for the construction of two stereogenic axes via double atroposelective C–H arylation or further transformation of the products via axial-to-axial diastereoinduction. Additionally, the reaction mechanism and the chirality transfer process are elucidated by density functional theory calculations.

INTRODUCTION

As we know, C–C atropisomers, e.g., axially chiral biaryls, are prevalent and privileged frameworks, and their construction has been well developed in the past decades.[1–4] C–N atropisomers, the siblings of C–C atropisomers, are also commonly found in bioactive natural products,[5] medicinal chemistry,[6] and recently in asymmetric catalysis as chiral ligands[7] (Figure 1A). However, compared with that of well-developed C–C atropisomers, the construction of C–N atropisomers has been less explored, which is probably due to the innate higher degree of rotational freedom and lower rotation barrier around a C–N bond.[3,8–10] In 2002, the Taguchi[11] and Curran[12] groups independently reported the first asymmetric syntheses of atropisomeric anilides through a palladium (Pd)-catalyzed N-allylation reaction, albeit with unsatisfied enantioselectivities. Since then, a number of catalytic asymmetric approaches have been developed for accessing these synthetically challenging skeletons (Figure 1B). Excellent stereoselectivities were obtained by means of N–H functionalization of anilides, including Pd-catalyzed N-arylation (Buchwald-Hartwig amination),[13,14] intramolecular Ullmann-type amination,[15] phase-transfer-catalyzed N-alkylation,[16] and cinchona alkaloid-catalyzed N-allylation.[17–19] Efficient approaches to directly constructing the atropisomeric C–N bond were also developed.[20–23] Other effective means included assembling the C–N atropisomers via *de novo* construction of the aromatic ring[24–27] and desymmetrization of prochiral anilides.[28–31] Recently, enantioselective C–H bond functionalization has emerged

The bigger picture

Axial chirality widely exists in bioactive natural products, pharmaceuticals, chiral materials, and chiral ligands and catalysts in asymmetric catalysis. As such, the efficient, modular, and enantioselective assembly of these scaffolds from readily available starting materials represents one of the most challenging yet fascinating directions in synthetic organic chemistry. In sharp contrast to the well-developed C–C axial chirality, atroposelective construction of C–N axial chirality has been less investigated because of the innate higher degree of rotational freedom of the latter. Herein, we report an efficient atroposelective construction of C–N atropisomers via palladium/chiral norbornene cooperative catalysis. The key to success is the unique axial-to-axial chirality transfer process, which has been scarcely reported. This strategy is expected to inspire future studies in asymmetric synthesis and find applications in broad research fields.

Please cite this article in press as: Liu et al., An axial-to-axial chirality transfer strategy for atroposelective construction of C–N axial chirality, Chem (2021), https://doi.org/10.1016/j.chempr.2021.04.005

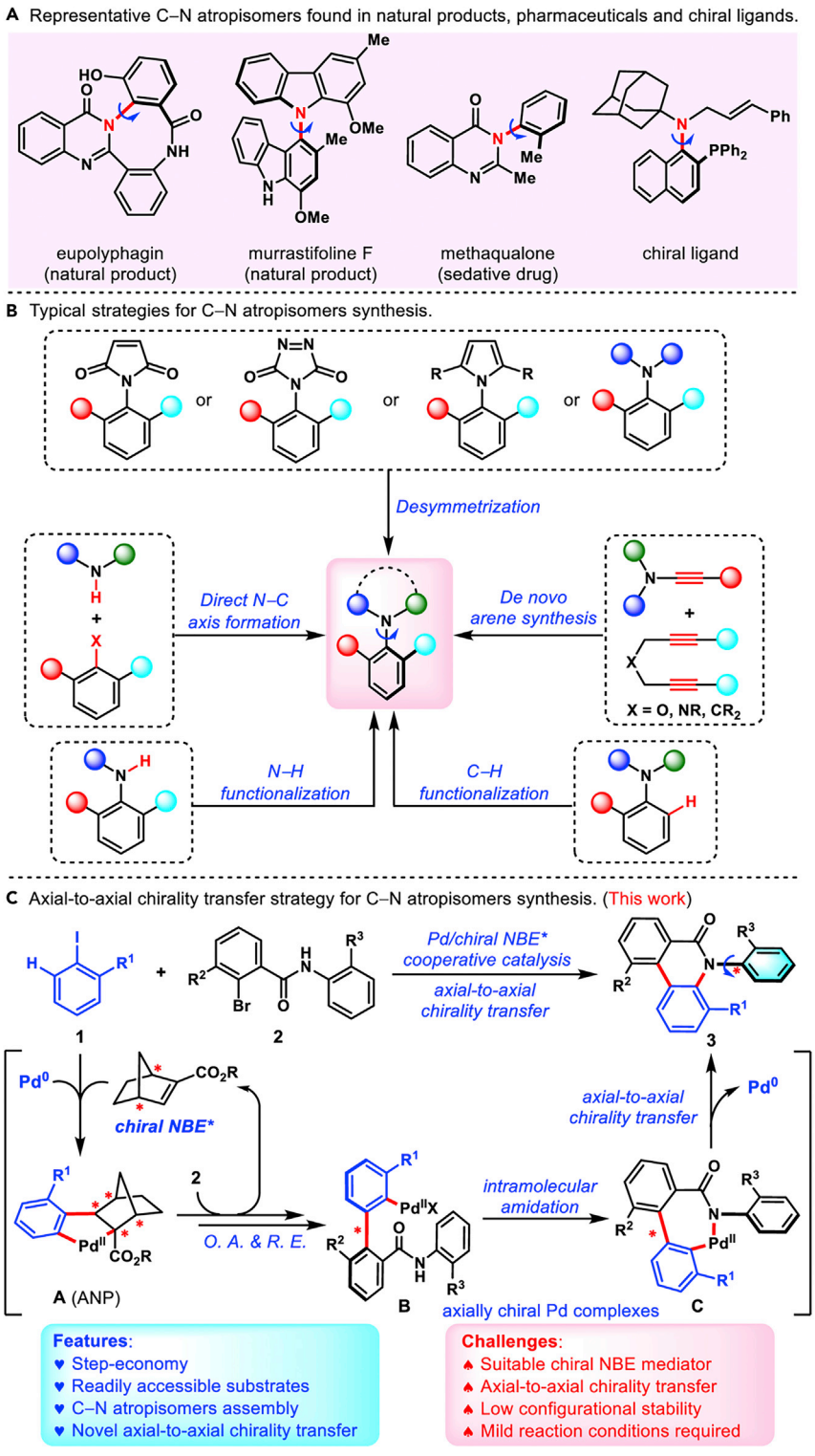

Figure 1. Representative C–N atropisomers and their synthetic strategies

as a powerful approach to constructing C–N axial chirality.[32–37] Despite these significant achievements, there is still room for improvement with regard to reaction efficiency, substrate generality, and product diversity. Therefore, developing more

[1]Sauvage Center for Molecular Sciences, Engineering Research Center of Organosilicon Compounds & Materials (Ministry of Education), College of Chemistry and Molecular Sciences, and Institute for Advanced Studies, Wuhan University, Wuhan 430072, China

[2]Department of Chemistry, Zhejiang University, Hangzhou 310058, China

[3]State Key Laboratory of Clean Energy Utilization, Zhejiang University, Hangzhou 310027, China

[4]These authors contributed equally

[5]Lead contact

*Correspondence: hxchem@zju.edu.cn (X.H.), qhzhou@whu.edu.cn (Q.Z.)

https://doi.org/10.1016/j.chempr.2021.04.005

Please cite this article in press as: Liu et al., An axial-to-axial chirality transfer strategy for atroposelective construction of C–N axial chirality, Chem (2021), https://doi.org/10.1016/j.chempr.2021.04.005

versatile and straightforward methods by using readily available starting materials to construct enantiopure C–N axial chirality is a highly desirable yet challenging task.

Palladium/norbornene (Pd/NBE) cooperative catalysis, namely the Catellani reaction,[38] enables simultaneous functionalization at both *ortho*- and *ipso*-positions of aryl halides, offering an efficient approach for polysubstituted arenes.[39–44] Recently, our group developed a general method to access C–C atropisomers via Pd/chiral NBE* cooperative catalysis.[45] On the basis of this chemistry, we envisioned a unique axial-to-axial chirality transfer strategy for C–N axial chirality construction via a preformed transient C–C axial chirality. As shown in Figure 1C, simple aryl iodide (**1**) is used as the substrate, and readily available 2,6-disubstituted aryl bromide with a tethered amide group (**2**) is utilized as both the arylating and terminating reagents. The process of oxidative addition, chiral NBE* insertion, and C–H activation leads to chiral aryl-NBE* palladacycle (ANP) complex **A**, which is then oxidized by aryl bromide **2**. The resulting Pd^{IV} complex subsequently undergoes reductive elimination and β-carbon elimination to form the key intermediate: axially chiral Pd complex **B**. Complex **B** eventually leads to the final product phenanthridinone **3** via intermediate **C**, which involves the intramolecular amidation to afford the desired C–N axially chiral phenanthridinone **3** alongside the chirality transfer from the C–C axis (**B** and **C**) to the C–N axis (**3**). Although it is strategically promising, several challenges need to be addressed. First, the identification of a suitable chiral NBE* mediator to ensure both good reactivity and enantioselectivity is crucial. However, to date, Pd/chiral NBE* cooperative catalysis has been rarely studied.[45–49] Second, the envisaged axial-to-axial chirality transfer should occur with high fidelity to preserve enantiopurity of the products. As we know, chirality transfer strategies, such as central-to-central, central-to-axial, and axial-to-central transfer, have already become excellent tools for the control of stereochemistry in asymmetric synthesis.[50–53] Surprisingly, axial-to-axial chirality transfer has been scarcely reported, and the factors that control this unique process remain largely unexplored, which we believe is owing to the innate dynamic nature of axial chirality.[54,55] Therefore, it is highly challenging yet encouraging to demonstrate the axial-to-axial chirality transfer strategy in a general way. Lastly, the reaction has to be performed under mild reaction conditions to avoid the potential racemization of C–N atropisomers because of their configurational vulnerability.

RESULTS AND DISCUSSION

To test our hypothesis, we initiated our studies with a model reaction by using simple 2-iodotoluene (**1a**) and 2,6-disubstituted aryl bromide (**2a**) as the reactants (Figure 2). To our delight, under the reported reaction conditions[45]—$Pd(OAc)_2$ as the catalyst, (1*S*,4*R*)-2-ethyl-ester-substituted chiral NBE* (N^{1*} [99% ee]) as the chiral mediator, and heating at 105°C—the desired C–N axially chiral phenanthridinone **3a** was indeed obtained with excellent yield (95%), albeit in only 24% ee. This preliminary result indicates that our previous design is feasible. The low enantioselectivity of **3a** was probably due to its low configurational stability at a high reaction temperature (105°C). After extensive optimization of the reaction parameters, including lowering the reaction temperature to 70°C (see Table S1 for details), the desired C–N axially chiral phenanthridinone **3a** was afforded with excellent yield and enantioselectivity (91% yield, 92% ee) under the optimal reaction conditions (Figure 2, entry 1). Control experiments were subsequently conducted to elucidate the role of each component of the reaction conditions. Not surprisingly, the Pd catalyst, chiral NBE* mediator, phosphine ligand, and base were all essential for this transformation (entries 2–5). The use of $PdCl_2$ instead of $Pd(OAc)_2$ resulted in a dramatically

Please cite this article in press as: Liu et al., An axial-to-axial chirality transfer strategy for atroposelective construction of C–N axial chirality, Chem (2021), https://doi.org/10.1016/j.chempr.2021.04.005

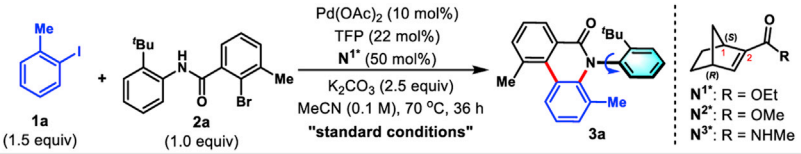

Entry[a]	Change from the standard conditions	Yield (%)[b]	Ee (%)[c]
1	none	94 (91)[d]	92
2	no $Pd(OAc)_2$ and TFP	0	--
3	no TFP	3	52
4	no $\mathbf{N^{1*}}$	0	--
5	no K_2CO_3	0	--
6	$PdCl_2$ instead of $Pd(OAc)_2$	31	84
7	PPh_3 instead of TFP	29	75
8	$\mathbf{N^{2*}}$ instead of $\mathbf{N^{1*}}$	76	90
9	$\mathbf{N^{3*}}$ instead of $\mathbf{N^{1*}}$	65	22
10	Cs_2CO_3 instead of K_2CO_3	54	91
11	DMF instead of MeCN	92	90
12[e]	25 mol% of $\mathbf{N^{1*}}$	92	90

Figure 2. Selected optimization of reaction conditions

[a]All reactions were performed on a 0.1 mmol scale.
[b]GC yield with biphenyl as an internal standard.
[c]Determined by chiral HPLC analysis.
[d]Isolated yield in parentheses.
[e]MeCN (0.2 M), 48 h.

decreased yield and enantioselectivity (entry 6). Tri(2-furyl)phosphine (TFP) is a better ligand than PPh_3 in terms of both reaction efficiency and enantioselectivity (entry 7). When the methyl ester-substituted chiral NBE* ($\mathbf{N^{2*}}$) was used instead of $\mathbf{N^{1*}}$, the yield of **3a** dropped to 76% (entry 8). The C2-amide substituted NBE* ($\mathbf{N^{3*}}$) proved to be an inferior mediator in terms of both yield and stereoselectivity (entry 9). When the stronger base Cs_2CO_3 was used instead of K_2CO_3, the yield decreased dramatically (entry 10). Besides MeCN, DMF was also a suitable solvent (entry 11). Notably, the loading of $\mathbf{N^{1*}}$ could be reduced to 25 mol % without obvious erosion of the reaction yield and enantioselectivity, although higher reaction concentration and longer reaction time were required (entry 12).

With the optimal reaction conditions in hand, we first set out to explore the reaction scope of aryl iodides (**1**) (Figure 3). In principle, aryl iodides with different electronic properties were all well tolerated, providing the desired axially chiral phenanthridinones in moderate to high yields (42%–96%) and good enantioselectivities (87%–98% ee) (Figure 3). A variety of *ortho*-substituents in aryl iodides were compatible, such as ethyl (**3b**), *tert*-butyldimethylsilyl (TBS)-protected hydroxymethyl (**3c**), ester (**3d**), phenyl (**3e**), fluoro (**3f**), benzyloxy (**3g**), and methoxy (**3h**). Moreover, aryl iodides bearing additional substituents at other positions were also examined, and it was found that alkyl (**3i** and **3k**), fluoro (**3l**), chloro (**3j**), bromo (**3m**), ester (**3n**), and amide (**3o**) groups at 3- or 4-positions were all amenable. In addition, bicyclic (**3s–3u**) and polycyclic (**3v**) aryl iodides were also investigated, and they afforded the desired products with excellent enantioselectivities (91%–96% ee). The use of densely functionalized aryl iodide substrates led to *penta*-substituted aromatics (**3w** and **3x**) with moderate yields. Moreover, heteroaryl iodide **1y** was also a suitable substrate to deliver **3y** in 50% yield and 96% ee. Remarkably, *meta*-substituted aryl iodides, which used to be problematic substrates in Catellani-type arylation reactions,[44]

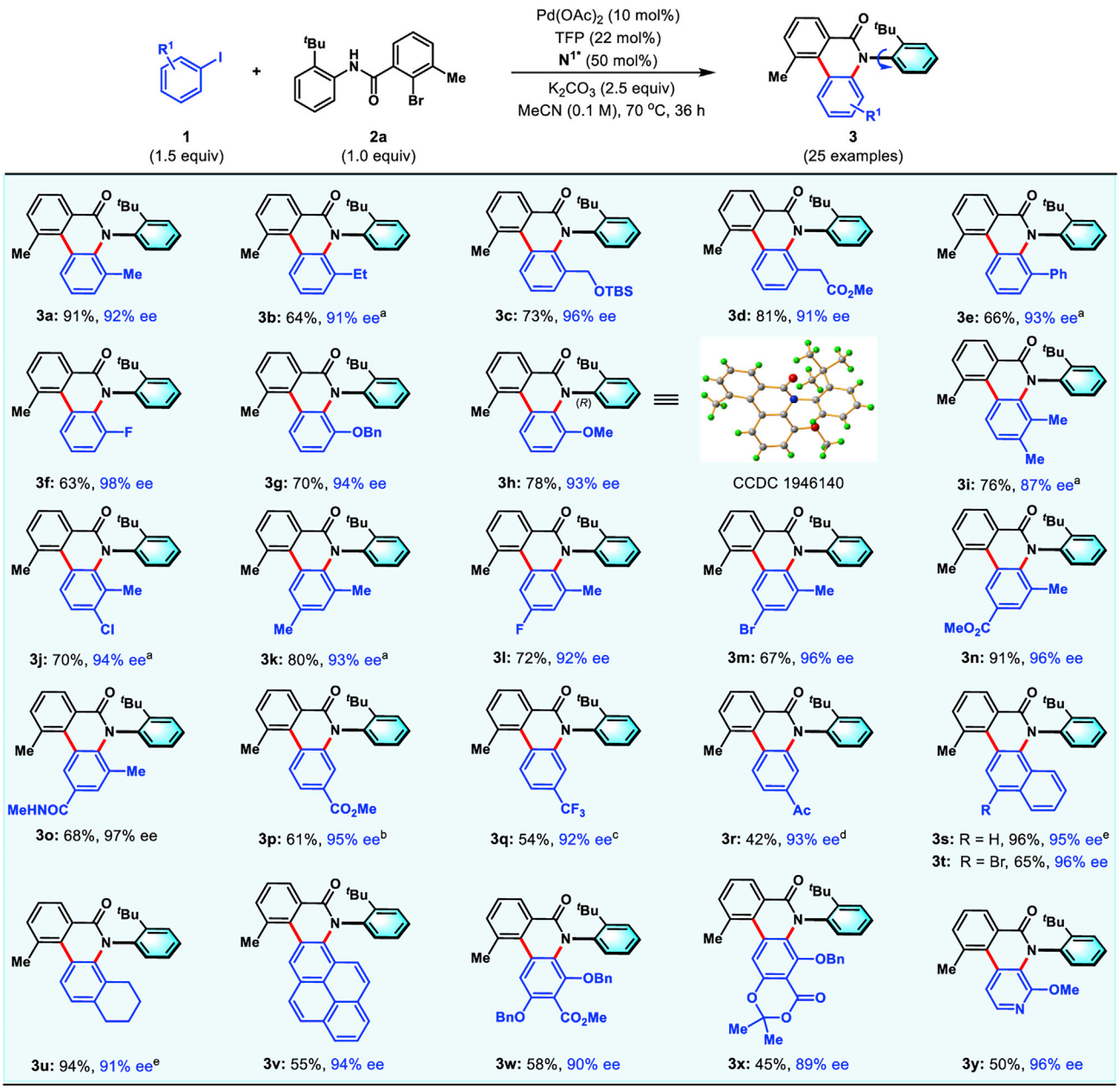

Figure 3. Substrate scope with respect to aryl iodides

All reactions were performed on a 0.1 mmol scale. Isolated yields are reported.

[a]60°C for 45 h.

[b]60°C for 60 h.

[c]75°C for 30 h.

[d]48 h.

[e]24 h.

provided the mono C–H arylated products (**3p**–**3r**) with excellent regioselectivity and stereocontrol.

Subsequently, the reaction scope of aryl bromides (**2**) was evaluated (Figure 4). Besides the methyl group, the *ortho*-substitution of aryl bromides can be extended to other functional groups, e.g., chloro (**3A**), nitro (**3B**), and naphthyl (**3C**), providing the

Please cite this article in press as: Liu et al., An axial-to-axial chirality transfer strategy for atroposelective construction of C–N axial chirality, Chem (2021), https://doi.org/10.1016/j.chempr.2021.04.005

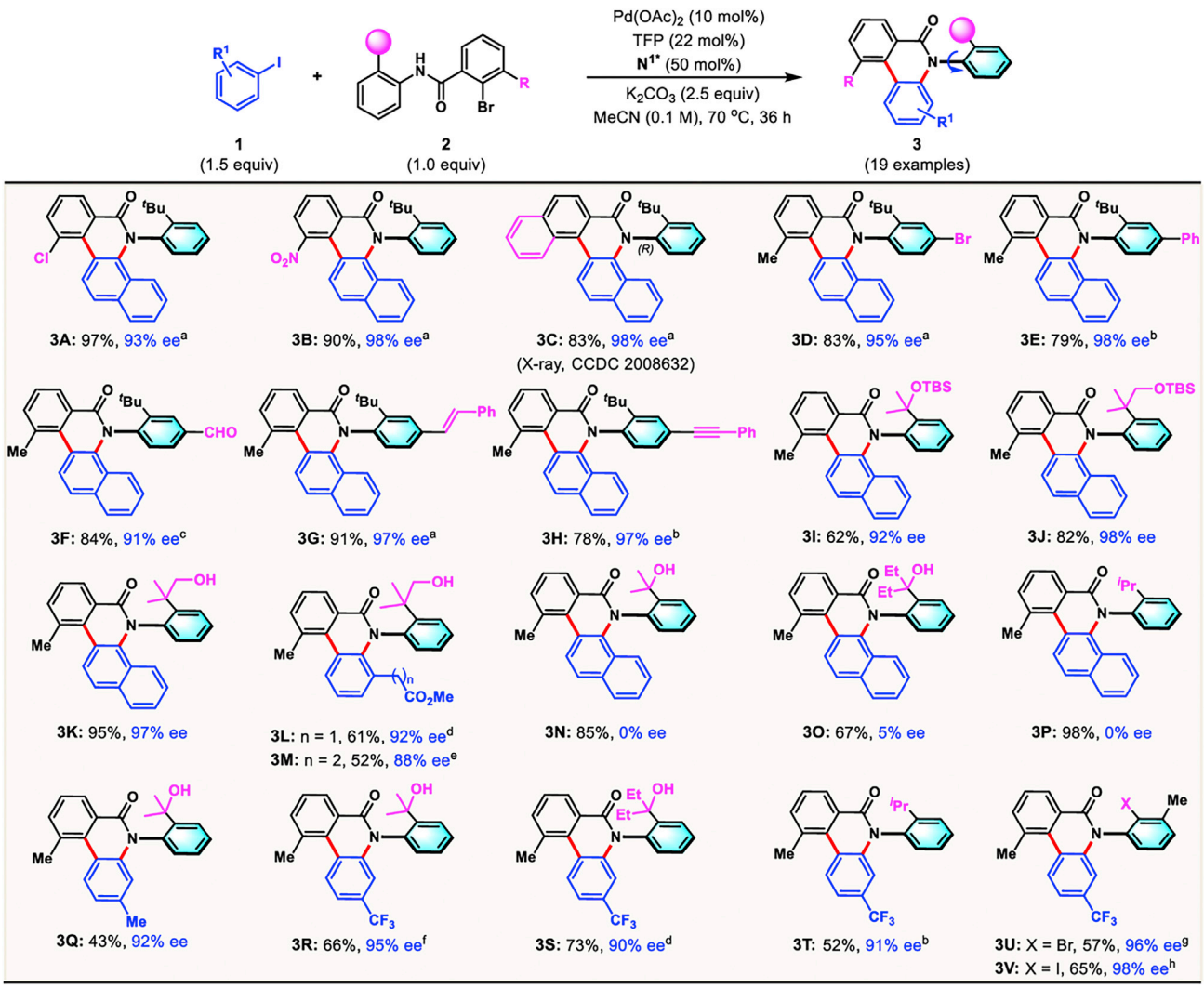

Figure 4. Substrate scope with respect to aryl bromides

All reactions were performed on a 0.1 mmol scale. Isolated yields are reported.

[a]24 h.

[b]60°C.

[c]60°C for 24 h.

[d]48 h.

[e]60 h.

[f]75°C.

[g]45°C for 72 h.

[h]50°C for 72 h.

corresponding products with excellent yields and enantioselectivities (83%–97% and 93%–98% ee). Modifications at the *para*-position of the aniline moiety of aryl bromides (**2**) were well tolerated, including bromo (**3D**), phenyl (**3E**), aldehyde (**3F**), alkenyl (**3G**), and alkynyl (**3H**). Notably, these functional groups can serve as useful synthetic handles for further chemical manipulations. In addition, modifications at the *ortho*-position of the aniline moiety were also investigated. In general, sterically bulky aniline moieties were required for ensuring high fidelity of the axial-to-axial chirality transfer process. Switching one methyl of the *tert*-butyl group to OTBS (**3I**), hydroxymethyl (**3K–3M**), or TBS-protected hydroxymethyl (**3J**)

Please cite this article in press as: Liu et al., An axial-to-axial chirality transfer strategy for atroposelective construction of C–N axial chirality, Chem (2021), https://doi.org/10.1016/j.chempr.2021.04.005

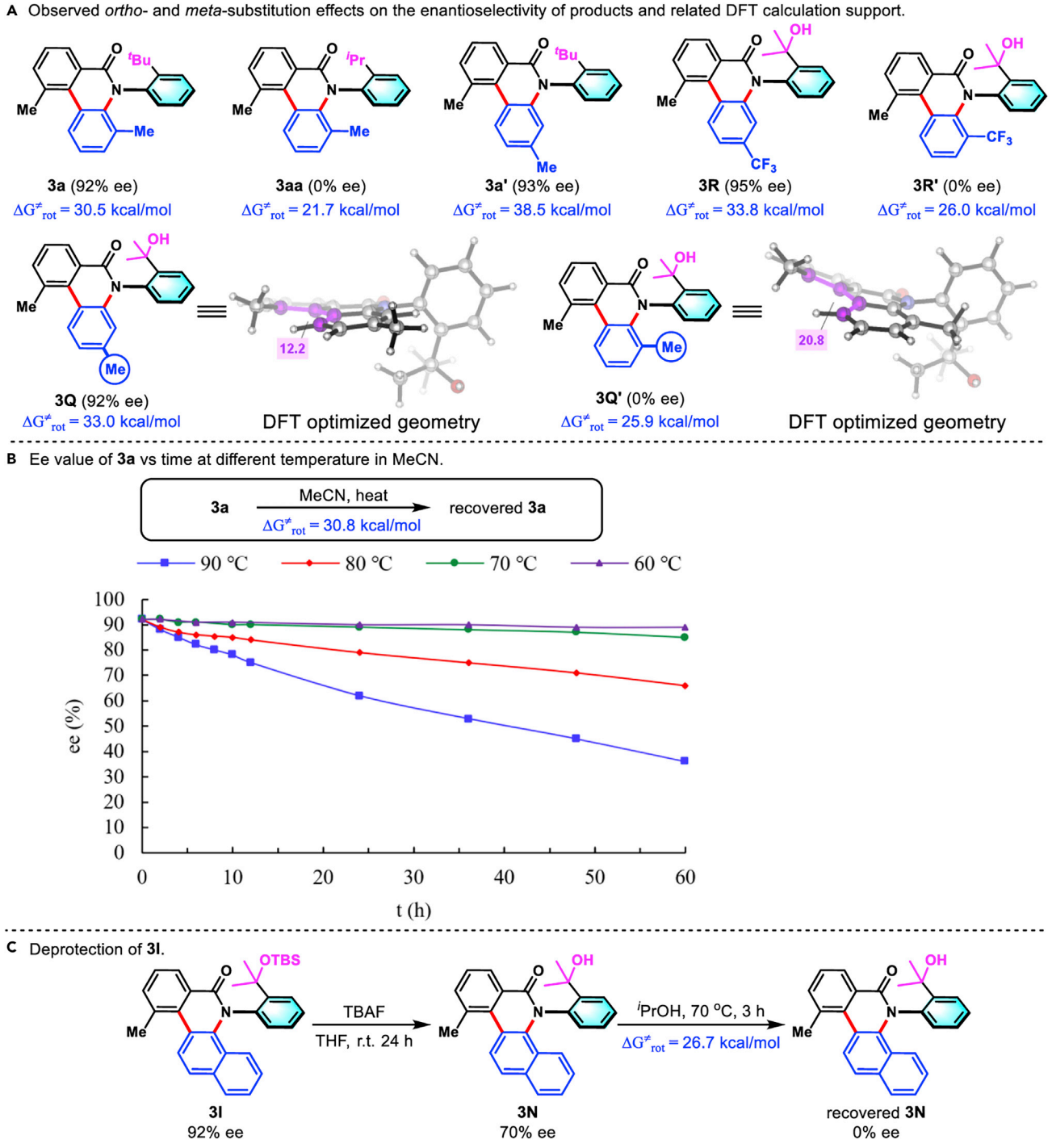

Figure 5. Observed *ortho*- and *meta*-substitution effects on the enantioselectivity and configurational stability of products and related DFT calculation support

produced the corresponding axially chiral phenanthridinones with good to excellent enantiocontrol. However, almost no enantioselectivities were observed when sterically less hindered aniline moieties were introduced (3N–3P). Nevertheless, when *meta*-substituted aryl iodides were used to react with these aryl bromides with a less bulky aniline moiety, the mono C–H arylated products (3Q–3V) were obtained

Please cite this article in press as: Liu et al., An axial-to-axial chirality transfer strategy for atroposelective construction of C–N axial chirality, Chem (2021), https://doi.org/10.1016/j.chempr.2021.04.005

with excellent regioselectivities and enantioselectivities (90%–98% ee). Particularly noteworthy is that the reaction also showed excellent chemoselectivity. When the arylation reagents contained two reactive C(sp^2)–X sites, the reaction selectively occurred at the C(sp^2)–X bond adjacent to the electron-withdrawing amide group (**3D**, **3U**, and **3V**). The absolute C–N axial configuration of both **3h** and **3C** was unambiguously determined to be (*R*) by X-ray crystallographic analysis, and that of the other products was assigned by analogy.

To understand the aforementioned interesting substituent effect on the rotation barrier and configurational stability of C–N axial chirality, we performed density functional theory (DFT) calculations (Figure 5A). Just as expected, reducing the size of the *ortho*-substituent at aniline moiety led to a lower rotation barrier (**3a** versus **3aa**). However, it was surprising to uncover that the *meta*-substitution at the aryl moiety from aryl iodide (blue part) significantly increased the rotation barrier of the corresponding C–N axis, as compared with that with the same substituent at the *ortho*-position (**3a′** versus **3a**, **3R** versus **3R′**, and **3Q** versus **3Q′**). We believe that this effect is related to the ground-state distortion with an *ortho*-substituent. The DFT-optimized structures of compounds **3Q** and **3Q′** are shown in Figure 5A. After the shift of methyl substitution from the *meta*- to *ortho*-position, the steric repulsions between this *ortho*-methyl substituent and the aryl group of the aniline moiety obviously distorted the ground-state structure, which was reflected at the significantly increased dihedral angle (12.2° versus 20.8°). This distortion destabilized the ground state, leading to a decreased rotation barrier (33.0 versus 25.9 kcal/mol). These interesting phenomena are consistent with the research by Kitagawa and coworkers, who also observed a significant decrease in the rotational barrier of C–N chiral axis due to distortion.[56] In addition, the rotation barrier of **3a** was experimentally measured ($\Delta G^{\neq}_{exp}$), and a satisfying consistency was observed as compared with the computational value ($\Delta G^{\neq}_{calc}$) ($\Delta G^{\neq}_{exp}$ = 30.8 kcal/mol and $\Delta G^{\neq}_{calc}$ = 30.5 kcal/mol; see Figures S1 and S2 for details).

To further investigate the configurational stability of the products, we performed racemization experiments (Figures 5B and 5C). First, we carefully monitored the ee values during the experiments of heating a solution of **3a** (92% ee) in MeCN at different temperatures (Figure 5B). We found that the C–N axis of **3a** with a 30.8 kcal/mol rotation barrier was stable only under 70°C, suggesting that these C–N atropisomers should be prepared under mild reaction conditions to avoid racemization. In addition, removal of the TBS group of **3I** (92% ee) with tetra-*n*-butylammonium fluoride (TBAF) at room temperature provided the deprotected product **3N** with only 70% ee (Figure 5C; see Scheme S3 for details). Further heating **3N** in isopropyl alcohol at 70°C for 3 h led to a complete racemization. The calculated rotation barrier of **3N** was 26.7 kcal/mol, which was consistent with the experimental results. These experiments indicate that the sterically bulky substituent at the *ortho*-position of aniline motif is essential to stabilizing the C–N axial configuration.

Next, we focused on illustrating the synthetic utilities of this method. First, we performed a scale-up experiment (3.0 mmol), which afforded 1.1 gram of the desired product **3C** without any erosion of the reaction efficiency and enantioselectivity, although a longer reaction time was required (Figure 6A). It is worth mentioning that the loading of $\mathbf{N}^{1*}$ in this experiment was reduced to 25 mol % with 71% recovery after workup. Then, aiming to assemble two stereogenic axes simultaneously, we performed an intriguing double atroposelective process (Figure 6B). The reaction of diiodides 4,4′-diiodo-3,3′-dimethyl-1,1′-biphenyl (**1aa**) and 1,5-diiodonaphthalene (**1ab**) with aryl bromide **2a** smoothly delivered the double C–H arylated products **3W** and **3Y** featuring two distal

Please cite this article in press as: Liu et al., An axial-to-axial chirality transfer strategy for atroposelective construction of C–N axial chirality, Chem (2021), https://doi.org/10.1016/j.chempr.2021.04.005

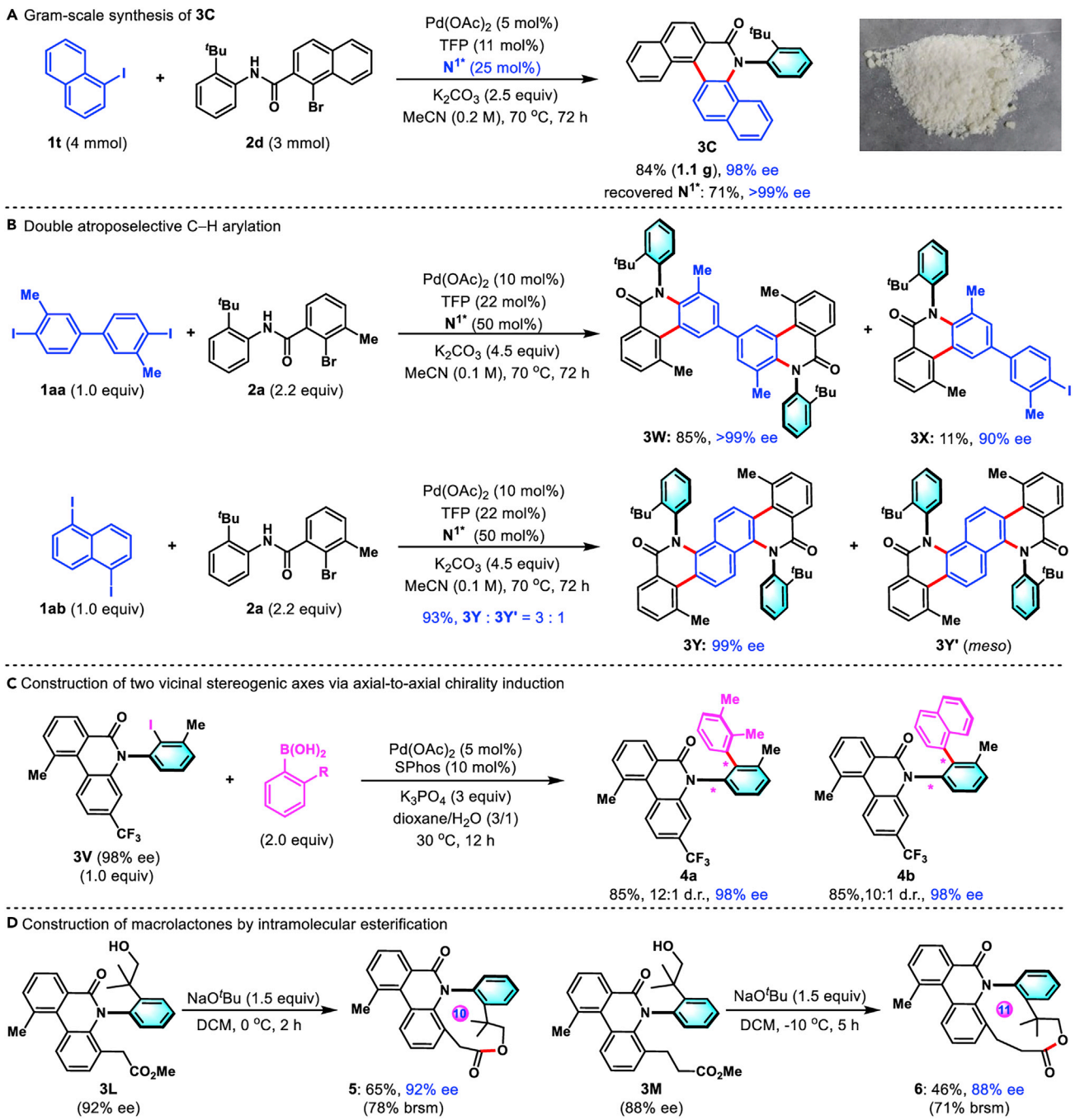

Figure 6. Synthetic applications

stereogenic C–N axes with excellent enantioselectivities.[57] When **1aa** was used as the substrate, the single C–N coupling product **3X** was also formed in 11% yield and 90% ee. When **1ab** was used, both **3Y** and its *meso*-isomer **3Y′** were obtained in a 3:1 ratio. Because the obtained C–N atropisomeric products are very useful intermediates, their appealing synthetic applications were also demonstrated. For example, product **3V** could be readily coupled with arylboronic acids under very mild conditions[58] without any erosion of enantioselectivity (Figure 6C). The products (**4a** and **4b**) uniquely possessing two vicinal C–N and C–C stereogenic axes were obtained with satisfactory

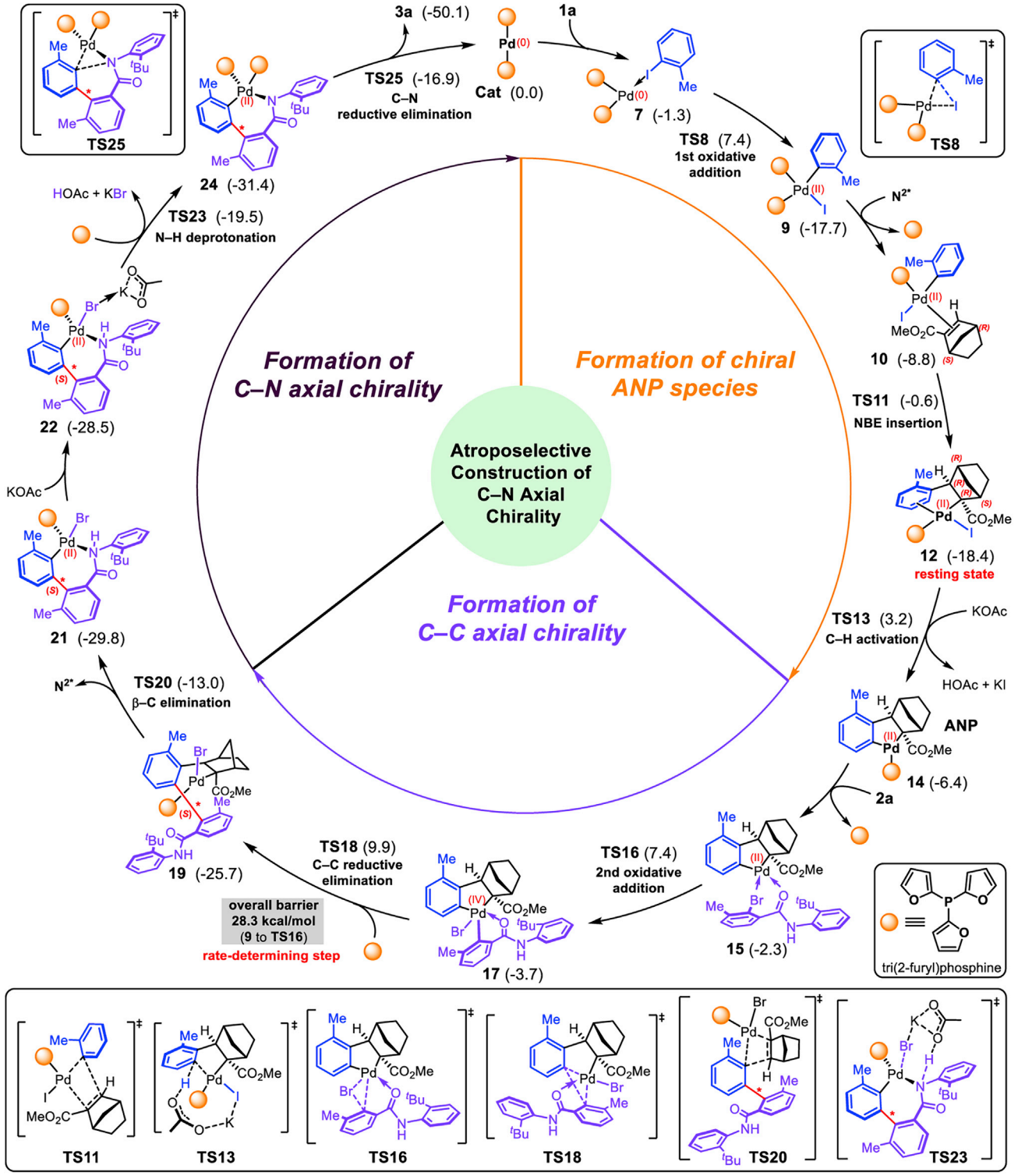

Figure 7. DFT-computed free-energy changes of the catalytic cycle of Pd/chiral NBE*-catalyzed construction of C–N atropisomers via the computational method of M06/6-311+G(d,p)-SDD-SMD(acetonitrile)//B3LYP-D3(BJ)/6-31G(d)-LANL2DZ

All free energies are in kcal/mol.

Please cite this article in press as: Liu et al., An axial-to-axial chirality transfer strategy for atroposelective construction of C–N axial chirality, Chem (2021), https://doi.org/10.1016/j.chempr.2021.04.005

diastereoselectivities (10–12:1 diastereomeric ratio [d.r.]). The absolute configuration of the newly formed C–C axis of **4a**, dictated by the proximal chiral C–N axis through an unconventional axial-to-axial diastereoinduction process, was assigned to be (*S*) by nuclear Overhauser effect (NOE) spectroscopy experiments (see Figure S3 for details). The overall process constituted a serial axial-to-axial chirality transfer and axial-to-axial stereoinduction event.[59] Finally, a facile treatment of products **3L** and **3M** with sodium *tert*-butoxide smoothly triggered an intramolecular esterification to deliver the 10- and 11-membered macrolactones embedded with a chiral C–N axis[60] (**5** and **6**) in 65% and 46% yields, respectively (Figure 6D).

To probe the reaction mechanism and the origins of enantioselectivity, we conducted DFT calculations on the basis of the previous mechanistic studies on Catellani-type reactions.[61,62] The free-energy changes of the operative catalytic cycle are shown in Figure 7. From the bisligated Pd(0) species **Cat**, the oxidative addition of aryl iodide **1a** occurred via **TS8**, generating the aryl Pd(II) intermediate **9**. Subsequent insertion of chiral NBE $\mathbf{N^{2*}}$ via **TS11** produced the alkylated Pd(II) intermediate **12**. Intermediate **12** underwent a base-assisted arene C–H bond activation via **TS13**, leading to ANP intermediate **14**. From **14**, the ligand exchange between aryl bromide **2a** and phosphine ligand led to the intermediate **15**, which then underwent the secondary oxidative addition via **TS16** to generate the Pd(IV) intermediate **17**. The subsequent reductive elimination produced the intermediate **19** with C–C axial chirality between the two aryl fragments. From **19**, the β-carbon elimination through **TS20** generated the intermediate **21** and released the chiral NBE* $\mathbf{N^{2*}}$. **21** then underwent the base-assisted N–H deprotonation via **22** to produce the amino Pd(II) intermediate **24**, which eventually underwent C–N reductive elimination via **TS25** to produce the observed product **3a** and regenerated the active Pd(0) catalyst. The complete DFT-computed free-energy profile is included in Figures S5 and S6. On the basis of our calculations, intermediate **12** was the on-cycle resting state. The rate-determining step was the C–C reductive elimination via **TS18**, which compared with **12**, required an overall barrier of 28.3 kcal/mol. The computations on alternative mechanistic considerations are included in the supplemental information.

The overall enantioselectivity of a C–N atropisomer product is determined by a series of stereoselectivity-controlling steps, which are elaborated in Figure 8. Figure 8A presents the DFT-computed free-energy changes of the catalytic cycle and the chirality transfer process from chiral NBE* ($\mathbf{N^{2*}}$) to the final product **3a**. From the $\mathbf{N^{2*}}$-coordinated aryl Pd(II)iodide intermediate **10**, the regioisomeric NBE* insertion and subsequent C–H activation favor the formation of chiral ANP intermediate **14**. This selectivity is due to the intrinsic frontier orbital interaction between $\mathbf{N^{2*}}$ and aryl Pd(II). In the alkene insertion, the ester-substituted olefin acts as the electrophilic component, and the aryl group of Pd(II) complex is the nucleophilic component. The LUMO (lowest unoccupied molecular orbital) π* orbital of $\mathbf{N^{2*}}$ has a smaller distribution at the ester-substituted position, which leads to the intrinsic regioselectivity of the alkene insertion at the other position (Figure S7). Through this regioselective insertion step, the chirality transfers from $\mathbf{N^{2*}}$ to the ANP species **14** (the DFT-computed free-energy changes of the competing formations of chiral cyclometallated species [Figure S7] and a detailed discussion are included in the supplemental information). From the chiral ANP **14**, subsequent oxidative addition of aryl bromide and reductive elimination generate a series of C–C atropisomeric intermediates. This axial chirality control is dictated by the chirality induction of the chiral cyclometallated fragment. As revealed in Figure 8B, **TS18** is 8.5 kcal/mol more favorable than **TS34**, which indicates a strong preference for the formation of (*S*)-axial chirality. In

Please cite this article in press as: Liu et al., An axial-to-axial chirality transfer strategy for atroposelective construction of C–N axial chirality, Chem (2021), https://doi.org/10.1016/j.chempr.2021.04.005

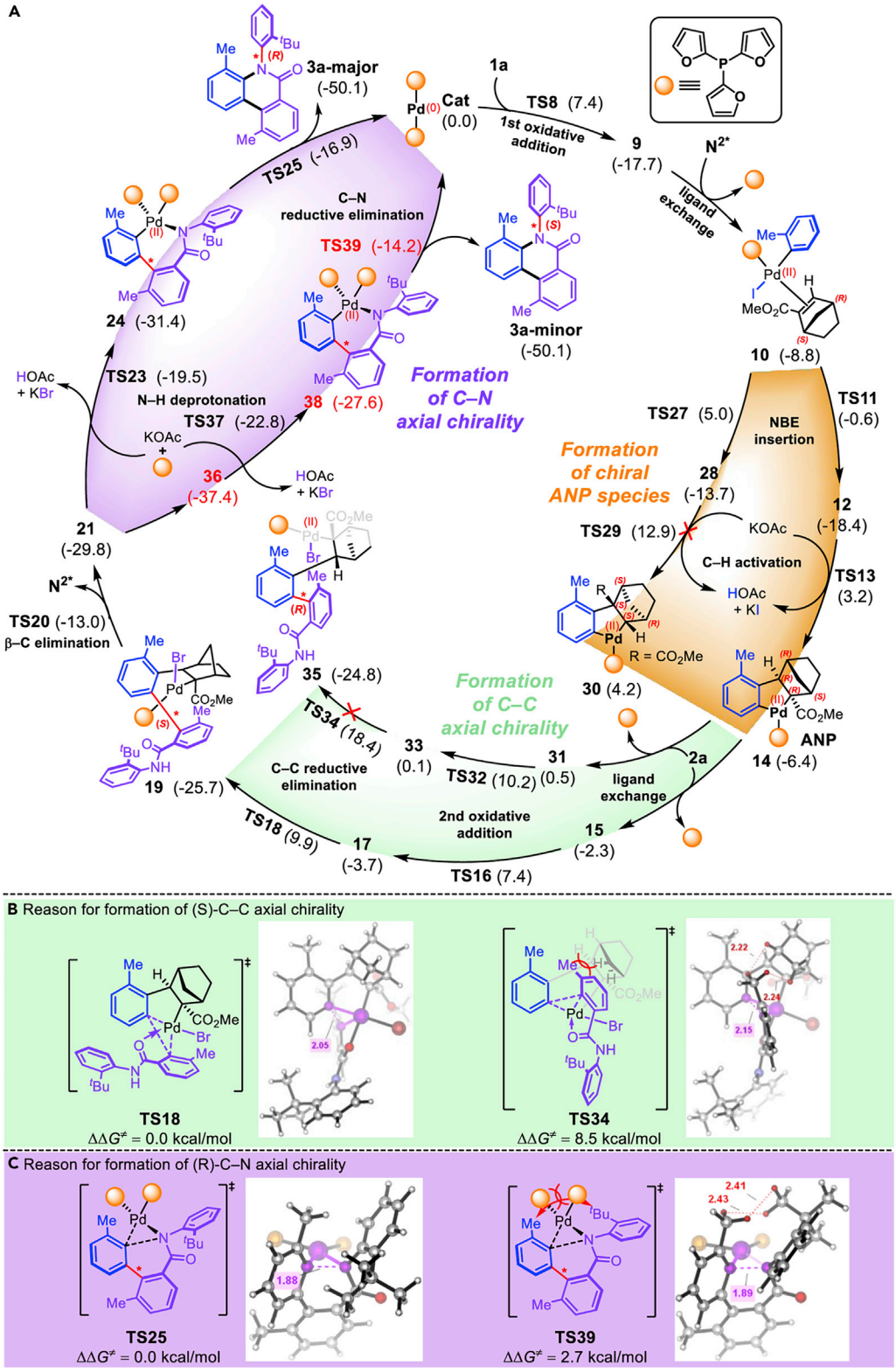

Please cite this article in press as: Liu et al., An axial-to-axial chirality transfer strategy for atroposelective construction of C–N axial chirality, Chem (2021), https://doi.org/10.1016/j.chempr.2021.04.005

Figure 8. Origins of chirality transfer process

(A) DFT-computed free-energy changes of the catalytic cycle of Pd/chiral NBE*-catalyzed construction of C–N atropisomers and the chiral transfer process. All free energies are in kcal/mol.

(B) DFT-optimized structures and the reason for formation of (*S*)-C–C axial chirality.

(C) DFT-optimized structures and the reason for formation of (*R*)-C–N axial chirality.

TS34, the aryl group from aryl bromide is proximal to the NBE* moiety, and the highlighted steric repulsions disfavor the subsequent C–C reductive elimination step of this transition state. In contrast, such steric repulsions do not exist in **TS18**, and thus the formation of intermediate **19** with (*S*)-axial chirality is favored (the DFT-computed free-energy changes for the competing formation of C–C atropisomers [Figure S8] and a detailed discussion are included in the supplemental information). Afterward, the preformed C–C axial chirality controls the formation of C–N axial chirality of final product **3a** through the irreversible C–N reductive elimination step. The competing C–N reductive elimination transition states **TS25** and **TS39** are shown in Figure 8C. The highlighted steric repulsions between the methyl group of the biaryl fragment with C–C axial chirality and the ^{t}Bu group of the amidyl fragment disfavor **TS39**, which results in a 2.7 kcal/mol preference for the formation of (*R*)-C–N axial chirality via **TS25** (the DFT-computed free-energy changes for the competing formation of C–N atropisomers [Figure S9] and a detailed discussion are included in the supplemental information).

These DFT calculations are in good agreement with the observed high level of axial-to-axial chirality transfer experimental results and the determined absolute C–N axial configurations by X-ray crystallographic analysis.

CONCLUSION

We have developed a modular and convergent method for atroposelective construction of C–N axial chirality through Pd/chiral NBE* cooperative catalysis. The strategy involves a unique axial-to-axial chirality transfer process. The obtained C–N axial chirality originates from the preformed transient C–C axial chirality with high fidelity. A wide range of C–N axially chiral phenanthridinones were obtained in good yields and excellent enantioselectivities. Other features include readily available starting materials, the ability to assemble two vicinal and remote stereogenic axes, high step economy, and scalability. DFT calculations revealed the reaction mechanism and the origins of high fidelity of the axial-to-axial chirality transfer process, providing broader implications for future studies in asymmetric synthesis.

EXPERIMENTAL PROCEDURES

Resource availability

Lead contact

Further information and requests for resources should be directed to and will be fulfilled by the lead contact, Qianghui Zhou (qhzhou@whu.edu.cn).

Materials availability

All materials generated in this study are available from the lead contact without restriction.

Data and code availability

The data of the X-ray crystallographic structures of **3h** and **3C** have been deposited in the Cambridge Crystallographic Data Center under accession numbers CCDC: 1946140 and 2008632.

Methods

Full experimental procedures are provided in the supplemental information.

SUPPLEMENTAL INFORMATION

Supplemental information can be found online at https://doi.org/10.1016/j.chempr.2021.04.005.

ACKNOWLEDGMENTS

We are grateful to the National Natural Science Foundation of China (21871213 and 22071189 to Q.Z., 21801193 to H.-G.C., and 21702182 and 21873081 to X.H.), the China Postdoctoral Science Foundation (2016M602339 to H.-G.C. and 2018M642894 to Z.-S.L.), Fundamental Research Funds for the Central Universities (2020XZZX002-02 to X.H.), the State Key Laboratory of Clean Energy Utilization (ZJUCEU2020007 to X.H.), and start-up funding from Wuhan University for financial support. Calculations were performed on the high-performance computing system at the Zhejiang University Department of Chemistry. We thank Prof. Wen-Bo Liu for sharing the instruments, Prof. Hengjiang Cong and Dr. Wei Yan for X-ray crystallographic analysis assistance, and Ms. Lisha Li and Mr. Hua Tang for technical assistance.

AUTHOR CONTRIBUTIONS

Q.Z. conceived the concept. Q.Z. and X.H. directed the project. Z.-S.L. made the initial discovery, performed the optimization, and explored the substrate scope and synthetic applications. Y.H., C.W., Y.M., J.C., and H.-G.C. conducted preparation of the starting materials and data analysis. P.-P.X. conducted the DFT calculations. Q.Z., X.H., Z.-S.L., and P.-P.X. wrote the paper with feedback from all other authors. Z.-S.L. and P.-P.X. contributed equally to this work.

DECLARATION OF INTERESTS

Q.Z. and Z.-S.L. have filed a provisional patent application (202110327590.9). All other authors declare no competing interests.

Received: February 3, 2021
Revised: March 11, 2021
Accepted: April 9, 2021
Published: May 13, 2021

REFERENCES

1. Liao, G., Zhou, T., Yao, Q.J., and Shi, B.F. (2019). Recent advances in the synthesis of axially chiral biaryls via transition metal-catalysed asymmetric C–H functionalization. Chem. Commun. *55*, 8514–8523.

2. Wang, Y.B., and Tan, B. (2018). Construction of axially chiral compounds via asymmetric organocatalysis. Acc. Chem. Res. *51*, 534–547.

3. Kumarasamy, E., Raghunathan, R., Sibi, M.P., and Sivaguru, J. (2015). Nonbiaryl and heterobiaryl atropisomers: molecular templates with promise for atropselective chemical transformations. Chem. Rev. *115*, 11239–11300.

4. Wencel-Delord, J., Panossian, A., Leroux, F.R., and Colobert, F. (2015). Recent advances and new concepts for the synthesis of axially stereoenriched biaryls. Chem. Soc. Rev. *44*, 3418–3430.

5. Bringmann, G., Tasler, S., Endress, H., Kraus, J., Messer, K., Wohlfarth, M., and Lobin, W. (2001). Murrastifoline-F: first total synthesis, atropo-enantiomer resolution, and stereoanalysis of an axially chiral N,C-coupled biaryl alkaloid. J. Am. Chem. Soc. *123*, 2703–2711.

6. Clayden, J., Moran, W.J., Edwards, P.J., and LaPlante, S.R. (2009). The challenge of atropisomerism in drug discovery. Angew. Chem. Int. Ed. *48*, 6398–6401.

7. Mino, T., Tanaka, Y., Hattori, Y., Yabusaki, T., Saotome, H., Sakamoto, M., and Fujita, T. (2006). Synthesis and optical resolution of aminophosphines with axially chiral C(aryl)–N(amine) bonds for use as ligands in asymmetric catalysis. J. Org. Chem. *71*, 7346–7353.

8. Kitagawa, O. (2021). Chiral Pd-catalyzed enantioselective syntheses of various N–C axially chiral compounds and their synthetic applications. Acc. Chem. Res. *54*, 719–730.

9. Li, Z., and Yu, S. (2020). Asymmetric synthesis of atropisomeric compounds with C–N chiral axis. Sci. Sin. Chim. *50*, 509–525.

10. Takahashi, I., Suzuki, Y., and Kitagawa, O. (2014). Asymmetric synthesis of atropisomeric compounds with an N–C chiral axis. Org. Prep. Proced. Int. *46*, 1–23.

11. Kitagawa, O., Kohriyama, M., and Taguchi, T. (2002). Catalytic asymmetric synthesis of optically active atropisomeric anilides through

enantioselective N-allylation with chiral Pd-tol-BINAP catalyst. J. Org. Chem. *67*, 8682–8684.

12. Terauchi, J., and Curran, D.P. (2003). N-Allylation of anilides with chiral palladium catalysts: the first catalytic asymmetric synthesis of axially chiral anilides. Tetrahedron: Asymmetry *14*, 587–592.

13. Kitagawa, O., Takahashi, M., Yoshikawa, M., and Taguchi, T. (2005). Efficient synthesis of optically active atropisomeric anilides through catalytic asymmetric N-arylation reaction. J. Am. Chem. Soc. *127*, 3676–3677.

14. Kitagawa, O., Yoshikawa, M., Tanabe, H., Morita, T., Takahashi, M., Dobashi, Y., and Taguchi, T. (2006). Highly enantioselective synthesis of atropisomeric anilide derivatives through catalytic asymmetric N-arylation: conformational analysis and application to asymmetric enolate chemistry. J. Am. Chem. Soc. *128*, 12923–12931.

15. Fan, X., Zhang, X., Li, C., and Gu, Z. (2019). Enantioselective atropisomeric anilides synthesis via Cu-catalyzed intramolecular adjacent C–N coupling. ACS Catal. *9*, 2286–2291.

16. Shirakawa, S., Liu, K., and Maruoka, K. (2012). Catalytic asymmetric synthesis of axially chiral o-iodoanilides by phase-transfer catalyzed alkylations. J. Am. Chem. Soc. *134*, 916–919.

17. Yang, G.-H., Zheng, H., Li, X., and Cheng, J.-P. (2020). Asymmetric synthesis of axially chiral phosphamides via atroposelective N-allylic alkylation. ACS Catal. *10*, 2324–2333.

18. Lu, S., Ng, S.V.H., Lovato, K., Ong, J.Y., Poh, S.B., Ng, X.Q., Kürti, L., and Zhao, Y. (2019). Practical access to axially chiral sulfonamides and biaryl amino phenols via organocatalytic atroposelective N-alkylation. Nat. Commun. *10*, 3061.

19. Li, S.L., Yang, C., Wu, Q., Zheng, H.L., Li, X., and Cheng, J.P. (2018). Atroposelective catalytic asymmetric allylic alkylation reaction for axially chiral anilides with achiral Morita-Baylis-Hillman carbonates. J. Am. Chem. Soc. *140*, 12836–12843.

20. Xia, W., An, Q.J., Xiang, S.H., Li, S., Wang, Y.B., and Tan, B. (2020). Chiral phosphoric acid catalyzed atroposelective C-H amination of arenes. Angew. Chem. Int. Ed. *59*, 6775–6779.

21. Frey, J., Malekafzali, A., Delso, I., Choppin, S., Colobert, F., and Wencel-Delord, J. (2020). Enantioselective synthesis of N–C axially chiral compounds by Cu-catalyzed atroposelective aryl amination. Angew. Chem. Int. Ed. *59*, 8844–8848.

22. Bai, H.Y., Tan, F.X., Liu, T.Q., Zhu, G.D., Tian, J.M., Ding, T.M., Chen, Z.M., and Zhang, S.Y. (2019). Highly atroposelective synthesis of nonbiaryl naphthalene-1,2-diamine N-C atropisomers through direct enantioselective C-H amination. Nat. Commun. *10*, 3063.

23. Brandes, S., Bella, M., Kjaersgaard, A., and Jørgensen, K.A. (2006). Chirally aminated 2-naphthols–organocatalytic synthesis of non-biaryl atropisomers by asymmetric Friedel-Crafts amination. Angew. Chem. Int. Ed. *45*, 1147–1151.

24. Wang, L., Zhong, J., and Lin, X. (2019). Atroposelective phosphoric acid catalyzed three-component cascade reaction: enantioselective synthesis of axially chiral N-arylindoles. Angew. Chem. Int. Ed. *58*, 15824–15828.

25. Zhang, L., Zhang, J., Ma, J., Cheng, D.J., and Tan, B. (2017). Highly atroposelective synthesis of arylpyrroles by catalytic asymmetric Paal-Knorr reaction. J. Am. Chem. Soc. *139*, 1714–1717.

26. Wang, Y.B., Zheng, S.C., Hu, Y.M., and Tan, B. (2017). Bronsted acid-catalysed enantioselective construction of axially chiral arylquinazolinones. Nat. Commun. *8*, 15489.

27. Tanaka, K., Takeishi, K., and Noguchi, K. (2006). Enantioselective synthesis of axially chiral anilides through rhodium-catalyzed [2+2+2] cycloaddition of 1,6-diynes with trimethylsilylynamides. J. Am. Chem. Soc. *128*, 4586–4587.

28. Gu, X.W., Sun, Y.L., Xie, J.L., Wang, X.B., Xu, Z., Yin, G.W., Li, L., Yang, K.F., and Xu, L.W. (2020). Stereospecific Si–C coupling and remote control of axial chirality by enantioselective palladium-catalyzed hydrosilylation of maleimides. Nat. Commun. *11*, 2904.

29. Zhang, J.W., Xu, J.H., Cheng, D.J., Shi, C., Liu, X.Y., and Tan, B. (2016). Discovery and enantiocontrol of axially chiral urazoles via organocatalytic tyrosine click reaction. Nat. Commun. *7*, 10677.

30. Zhang, J., Zhang, Y., Lin, L., Yao, Q., Liu, X., and Feng, X. (2015). Catalytic asymmetric desymmetrization of N-arylmaleimides: efficient construction of both atom chirality and axial chirality. Chem. Commun. *51*, 10554–10557.

31. Di Iorio, N., Righi, P., Mazzanti, A., Mancinelli, M., Ciogli, A., and Bencivenni, G. (2014). Remote control of axial chirality: aminocatalytic desymmetrization of N-arylmaleimides via vinylogous Michael addition. J. Am. Chem. Soc. *136*, 10250–10253.

32. Yao, Q.J., Xie, P.P., Wu, Y.J., Feng, Y.L., Teng, M.Y., Hong, X., and Shi, B.F. (2020). Enantioselective synthesis of atropisomeric anilides via Pd(II)-catalyzed asymmetric C–H olefination. J. Am. Chem. Soc. *142*, 18266–18276.

33. Ye, C.X., Chen, S., Han, F., Xie, X., Ivlev, S., Houk, K.N., and Meggers, E. (2020). Atroposelective synthesis of axially chiral N-arylpyrroles by chiral-at-rhodium catalysis. Angew. Chem. Int. Ed. *59*, 13552–13556.

34. Zhang, S., Yao, Q.-J., Liao, G., Li, X., Li, H., Chen, H.-M., et al. (2019). Enantioselective synthesis of atropisomers featuring pentatomic heteroaromatics by Pd-catalyzed C–H alkynylation. ACS Catal. *9*, 1956–1961.

35. Li, H., Yan, X., Zhang, J., Guo, W., Jiang, J., and Wang, J. (2019). Enantioselective synthesis of C–N axially chiral N-aryloxindoles by asymmetric rhodium-catalyzed dual C–H activation. Angew. Chem. Int. Ed. *58*, 6732–6736.

36. Diener, M.E., Metrano, A.J., Kusano, S., and Miller, S.J. (2015). Enantioselective synthesis of 3-arylquinazolin-4(3H)-ones via peptide-catalyzed atroposelective bromination. J. Am. Chem. Soc. *137*, 12369–12377.

37. Crawford, J.M., Stone, E.A., Metrano, A.J., Miller, S.J., and Sigman, M.S. (2018). Parameterization and analysis of peptide-based catalysts for the atroposelective bromination of 3-arylquinazolin-4(3H)-ones. J. Am. Chem. Soc. *140*, 868–871.

38. Catellani, M., Frignani, F., and Rangoni, A. (1997). A complex catalytic cycle leading to a regioselective synthesis of o,o′-disubstituted vinylarenes. Angew. Chem. Int. Ed. *36*, 119–122.

39. Wang, J., and Dong, G. (2019). Palladium/norbornene cooperative catalysis. Chem. Rev. *119*, 7478–7528.

40. Cheng, H.G., Chen, S., Chen, R., and Zhou, Q. (2019). Palladium(II)-initiated Catellani-type reactions. Angew. Chem. Int. Ed. *58*, 5832–5844.

41. Liu, Z.S., Gao, Q., Cheng, H.G., and Zhou, Q. (2018). Alkylating reagents employed in Catellani-type reactions. Chem. Eur. J. *24*, 15461–15476.

42. Della Ca', N., Fontana, M., Motti, E., and Catellani, M. (2016). Pd/norbornene: a winning combination for selective aromatic functionalization via C–H bond activation. Acc. Chem. Res. *49*, 1389–1400.

43. Ye, J., and Lautens, M. (2015). Palladium-catalysed norbornene-mediated C–H functionalization of arenes. Nat. Chem. *7*, 863–870.

44. Catellani, M., Motti, E., and Della Ca', N. (2008). Catalytic sequential reactions involving palladacycle-directed aryl coupling steps. Acc. Chem. Res. *41*, 1512–1522.

45. Liu, Z.-S., Hua, Y., Gao, Q., Ma, Y., Tang, H., Shang, Y., et al. (2020). Construction of axial chirality via palladium/chiral norbornene cooperative catalysis. Nat. Catal. *3*, 727–733.

46. Zhou, Q., Hua, Y., Liu, Z.S., Xie, P.P., Ding, B., Cheng, H.G., et al. (2021). Kinetic resolution of tertiary benzyl alcohols via palladium/chiral norbornene cooperative catalysis. Angew. Chem. Int. Ed. https://doi.org/10.1002/anie.202103428.

47. Feng, Q., Ma, X., Bao, W., Li, S.-J., Lan, Y., and Song, Q. (2021). Catalytic atroposelective Catellani reaction enables construction of axially chiral biaryl monophosphine oxides. CCS Chem. *3*, 377–387.

48. Shi, H., Herron, A.N., Shao, Y., Shao, Q., and Yu, J.Q. (2018). Enantioselective remote *meta*-C–H arylation and alkylation via a chiral transient mediator. Nature *558*, 581–585.

49. Li, R., Liu, F., and Dong, G. (2018). Palladium-catalyzed asymmetric annulation between aryl iodides and racemic epoxides using a chiral norbornene cocatalyst. Org. Chem. Front. *5*, 3108–3112.

50. Campolo, D., Gastaldi, S., Roussel, C., Bertrand, M.P., and Nechab, M. (2013). Axial-to-central chirality transfer in cyclization processes. Chem. Soc. Rev. *42*, 8434–8466.

51. Alonso, J.M., Quirós, M.T., and Muñoz, M.P. (2016). Chirality transfer in metal-catalysed intermolecular addition reactions involving allenes. Org. Chem. Front. *3*, 1186–1204.

52. Yang, H., Chen, J., and Zhou, L. (2020). Construction of axially chiral compounds via central-to-axial chirality conversion. Chem. Asian J. *15*, 2939–2951.

53. Nguyen, T.T. (2019). Traceless point-to-axial chirality exchange in the atropselective synthesis of biaryls/heterobiaryls. Org. Biomol. Chem. *17*, 6952–6963.

54. Mori, K., Ohmori, K., and Suzuki, K. (2009). Stereochemical relay via axially chiral styrenes: asymmetric synthesis of the antibiotic TAN-1085. Angew. Chem. Int. Ed. *48*, 5633–5637.

55. Liu, H., Feng, W., Kee, C.W., Leow, D., Loh, W.-T., and Tan, C.-H. (2010). Brønsted base-catalyzed tandem isomerization-Michael reactions of alkynes: synthesis of oxacycles and azacycles. Adv. Synth. Catal. *352*, 3373–3379.

56. Suzuki, Y., Takahashi, I., Dobashi, Y., Hasegawa, H., Roussel, C., and Kitagawa, O. (2015). Relationship between rotational barriers and structures in N–C axially chiral 3,4-dihydroquinolin-2-one and 3,4-dihydrobenzoquinolin-2-one. Tetrahedron Lett. *56*, 132–135.

57. Harned, A.M. (2018). From determination of enantiopurity to the construction of complex molecules: the Horeau principle and its application in synthesis. Tetrahedron *74*, 3797–3841.

58. Martin, R., and Buchwald, S.L. (2008). Palladium-catalyzed Suzuki-Miyaura cross-coupling reactions employing dialkylbiaryl phosphine ligands. Acc. Chem. Res. *41*, 1461–1473.

59. Park, K.H., Chen, R., and Chen, D.Y.-K. (2017). Programmed serial stereochemical relay and its application in the synthesis of morphinans. Chem. Sci. *8*, 7031–7037.

60. Parenty, A., Moreau, X., and Campagne, J.M. (2006). Macrolactonizations in the total synthesis of natural products. Chem. Rev. *106*, 911–939.

61. Maestri, G., Motti, E., Della Ca', N., Malacria, M., Derat, E., and Catellani, M. (2011). Of the Ortho effect in palladium/norbornene-catalyzed reactions: a theoretical investigation. J. Am. Chem. Soc. *133*, 8574–8585.

62. Chai, D.I., Thansandote, P., and Lautens, M. (2011). Mechanistic studies of Pd-catalyzed regioselective aryl C–H bond functionalization with strained alkenes: origin of regioselectivity. Chem. Eur. J. *17*, 8175–8188.